nature cell biology

XMAP215 activity sets spindle length by controlling the total mass of spindle microtubules

Simone B. Reber[1], Johannes Baumgart[2], Per O. Widlund[1], Andrei Pozniakovsky[1], Jonathon Howard[1,3], Anthony A. Hyman[1,4] and Frank Jülicher[2,4]

Metaphase spindles are microtubule-based structures that use a multitude of proteins to modulate their morphology and function. Today, we understand many details of microtubule assembly, the role of microtubule-associated proteins, and the action of molecular motors[1,2]. Ultimately, the challenge remains to understand how the collective behaviour of these nanometre-scale processes gives rise to a properly sized spindle on the micrometre scale. By systematically engineering the enzymatic activity of XMAP215, a processive microtubule polymerase[3,4], we show that *Xenopus laevis* spindle length increases linearly with microtubule growth velocity, whereas other parameters of spindle organization, such as microtubule density, lifetime and spindle shape, remain constant. We further show that mass balance can be used to link the global property of spindle size to individual microtubule dynamic parameters. We propose that spindle length is set by a balance of non-uniform nucleation and global microtubule disassembly in a liquid-crystal-like arrangement of microtubules.

The biological importance of organelle size has recently attracted a surge of interest[5–7]. In the case of the metaphase or postanaphase B spindle, length is particularly important as it determines the distance over which chromosomes are segregated. Although a few general principles of spindle length control are beginning to emerge, the relative contribution of microtubule dynamics, nucleation and transport to spindle size remains elusive[8–11].

Dynamic spindles assembled in *Xenopus* egg extracts are an excellent model system to study spindle organization[10–12]. The egg extract is an open system that permits biochemical manipulation and quantitative kinetic studies. It is void of cortical restrictions and spindle material is not limited[13], which allows us to study mechanisms of length control intrinsic to the spindle. *Xenopus* spindles are self-organizing ensembles of microtubules, which nucleate by different pathways[1], turn over rapidly[14], slide poleward[15] and are short when compared with the overall length of the spindle[11]. Although all of these processes are likely to influence spindle assembly, their interplay makes it challenging to establish direct links between individual parameters of microtubule dynamics and the overall spindle length.

Proteins of the XMAP215/Dis1 family are major regulators of microtubule polymerization[16]. Supporting the role of XMAP215 as a microtubule growth promoter, its depletion leads to shorter spindles or defects in spindle morphology in *Schizosaccharomyces pombe*, *Caenorhabditis elegans*, *Xenopus* egg extracts, *Drosophila melanogaster* and HeLa cells[17]. Members of the XMAP215/Dis1 family contain varying numbers of TOG (tumour overexpressed gene) domains that function as αβ-tubulin-binding modules[17]. Recent *in vitro* studies show that XMAP215 acts as a processive polymerase[4] and that its polymerase activity depends on tubulin binding to multiple TOG domains[18]. Mutation of conserved residues in different TOG domains reduces tubulin binding while concomitantly reducing the maximal growth-promoting activity of the polymerase. Combining mutations in different TOG domains (Fig. 1a) enables the construction of XMAP215 mutants characterized by significantly different maximum growth rates. This collection of engineered polymerases provides a valuable tool and allows us to study the contribution of microtubule polymerization dynamics to spindle morphology.

To determine the quantitative relation between polymerase activity and spindle length, we depleted endogenous XMAP215 from *Xenopus* egg extracts, added back green fluorescent protein (GFP)-tagged point mutants of XMAP215 to the endogenous concentration (Fig. 1b) and assembled spindles. All mutants, although having different affinities towards the tubulin heterodimer, localize to spindle microtubules (Supplementary Fig. S1a,b) and interact with XTACC3 (*Xenopus* transforming acidic coiled-coil protein 3) (Supplementary Fig. S1c), as previously reported for the wild-type protein[19]. These findings confirm the *in vitro* data suggesting that the introduced point mutations alter the polymerase activity of XMAP215 but no other of its characteristics.

[1]Max Planck Institute of Molecular Cell Biology and Genetics, Pfotenhauer Str. 108, 01307 Dresden, Germany. [2]Max Planck Institute for the Physics of Complex Systems, Nöthnitzer Str. 38, 01187 Dresden, Germany. [3]Present address: Department of Molecular Biophysics and Biochemistry, Yale University, New Haven, Connecticut 06520-8114, USA.
[4]Correspondence should be addressed to A.A.H. or F.J. (e-mail: hyman@mpi-cbg.de or julicher@pks.mpg.de)

Received 31 October 2012; accepted 24 July 2013; published online 25 August 2013; DOI: 10.1038/ncb2834

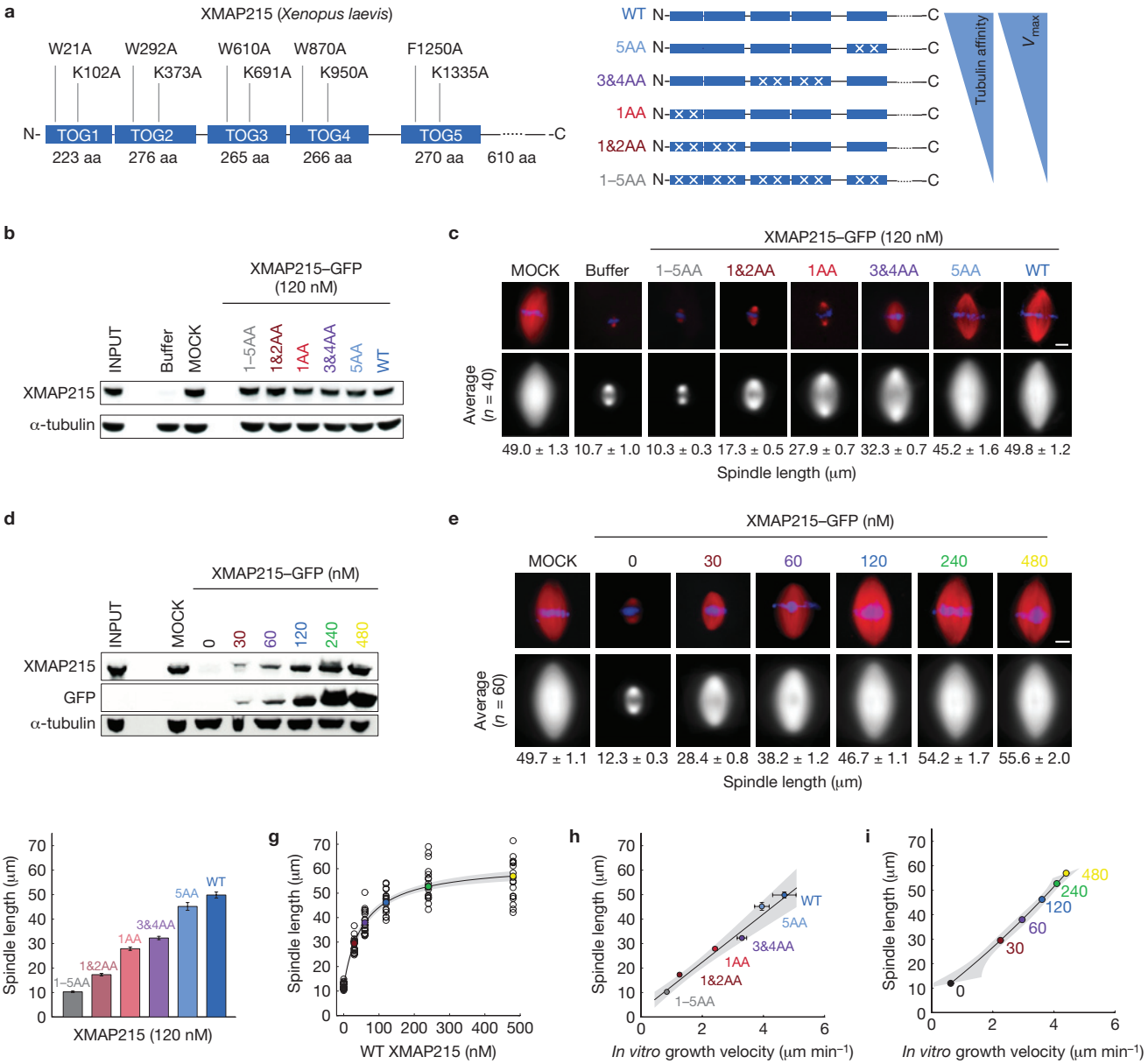

Figure 1 Spindle length is directly proportional to *in vitro* XMAP215 microtubule polymerase activity. (**a**) Schematic diagram of the domain structure of *Xenopus laevis* XMAP215 and the positions of the point mutations introduced. Summary of microtubule affinity and maximal growth promotion[18] for the mutants used in this study. (**b**–**e**) *Xenopus* egg extract was MOCK or XMAP215 depleted, and different point mutants of XMAP215–GFP or increasing concentrations of wild-type XMAP215–GFP were added back. Depletion efficiency and accuracy of add-back were controlled by western blot analysis; tubulin served as a loading control. Spindles were assembled in the presence of different XMAP215 mutants (at 120 nM) or increasing XMAP215 concentrations (0–480 nM). The upper rows show a representative spindle (red, microtubules; blue, DNA), the lower rows show an average image of all spindles, and the average spindle length (±s.e.m.) is indicated; (**c**) $n = 40$ spindles assessed over 3 independent experiments and (**e**) $n = 60$ spindles assessed over 3 independent experiments. Scale bars, 10 μm. (**f**) Average spindle length measured in the presence of different XMAP215–GFP point mutants. Error bars indicate s.e.m. ($n = 40$ spindles assessed over three independent experiments). (**g**) Spindle length was measured and plotted versus XMAP215–GFP concentration. Individual data points (open circles, $n = 20$ spindles, one representative data set of three independent experiments) were fitted with Michaelis–Menten kinetics; the grey area indicates the 95% confidence interval of the fitted function by weighted least squares. (**h**) Spindle length plotted versus the maximal *in vitro* microtubule growth velocity promoted by different XMAP215 mutants at 400 nM. Error bars indicate s.e.m. ($n_y = 40$ spindles assessed over 3 independent experiments; n_x = WT 11(2), 5AA 15(2), 3&4AA 11(2), 1AA 11(2), 1&2AA 15(2), 1–5AA no growth over tubulin alone. N_x, independent measurements of individual growth events. Number of independent experiments for each condition is given in parentheses). The grey area indicates the 95% confidence intervals of the fitted curves. (**i**) Spindle length plotted versus the maximal *in vitro* microtubule growth velocity promoted by increasing wild-type XMAP215 concentrations. The grey area indicates the 95% confidence intervals of the fitted curves.

When we added back XMAP215 TOG1-5AA–GFP, a mutant that no longer binds free tubulin and consequently does not promote microtubule growth *in vitro*[18], spindle assembly failed or only small spindles assembled (Fig. 1c), even at high TOG1-5AA concentrations (Supplementary Fig. S1d). Next, we added back mutants of XMAP215 that reduce the maximal growth-promoting activity of the polymerase

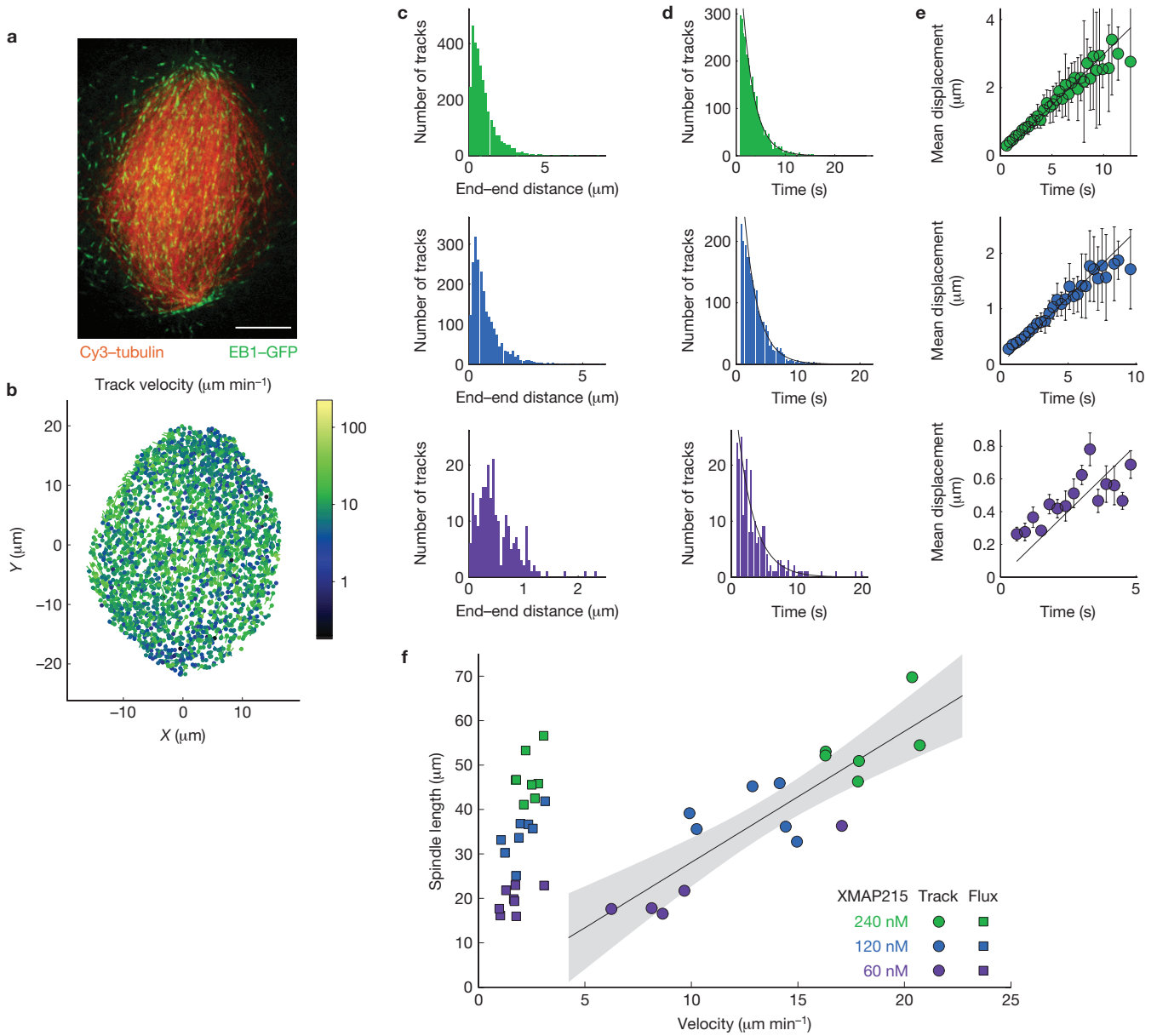

Figure 2 Spindle length scales with spindle microtubule growth velocity. (**a**) Spindle assembled in *Xenopus* egg extract (red: Cy3–tubulin, green: EB1–GFP). Scale bar, 10 μm. (**b**) All EB1–GFP tracks detected in a single time-lapse sequence (time resolution 0.3 s) of a wild-type *Xenopus* spindle. Total number of tracks: 2,752. The heat map colour codes for microtubule growth, the circle represents the start of the track, and the line its length. (**c**,**d**) Histograms of the distance (**c**) and time (**d**) EB1 tracks travelled in a spindle assembled at 240 nM (green, upper row), 120 nM (blue, middle row) and 60 nM (purple, bottom row) XMAP215. (**e**) The EB1–GFP tracks were binned by time and the average distance for each group was evaluated. The weighted linear fit without a constant to this evaluated distance versus time data provides the velocity at which the EB1–GFP tracks travel. Error bars indicate s.e.m., which is based on the corresponding bins shown in **d**. The total number of tracks for the representative spindle assembled at 60 nM XMAP215 (green): 138 tracks; at 120 nM XMAP215 (blue): 2,688 tracks; and at 240 nM XMAP215 (purple): 3,223 tracks. (**f**) Individual data points for spindle length versus EB1–GFP track velocity (circle) and flux velocity (square). The colour code indicates the XMAP215 concentration at which spindles were assembled. The grey area indicates the 95% confidence interval of the fitted curve.

over a 5.5-fold range, assembled spindles and measured their length (Fig. 1f). At the endogenous concentration, these mutants promoted assembly of spindles at lengths proportional to their polymerase activity. Similarly, spindle length increased with increasing wild-type XMAP215 concentrations (Fig. 1d,e). However, when adding more than 240 nM XMAP215–GFP, spindle length plateaued (Fig. 1g). We correlated spindle length with the maximum microtubule growth promotion of XMAP215 determined in total-internal-reflection fluorescence microscopy assays (Supplementary Fig. S1e,f). In both, the point mutant (Fig. 1h) and the dose–response (Fig. 1i) assay, spindle length is proportional to the maximal growth rate promoted by the polymerase XMAP215.

Next, we wanted to correlate spindle length with microtubule growth rates measured in spindles. Therefore, we added EB1–GFP, a (+) TIP-binding protein that tracks growing microtubule ends[20,21] and imaged spindles over time (Fig. 2a). In each spindle, microtubule plus ends

were automatically detected (Fig. 2b), microtubule growth events were tracked over consecutive frames and track length (Fig. 2c), duration (Fig. 2d) and growth velocities (Fig. 2e) were evaluated. The analysis of EB1–GFP tracks measured in control spindles revealed an average growth velocity of $12.8 \pm 0.9\,\mu m\,min^{-1}$ (s.e.m., $n = 6$ spindles). This velocity, however, does not represent microtubule growth velocities *per se* but the combined effect of microtubule flux[15], which occurs at a rate of approximately $2\,\mu m\,min^{-1}$, and growth velocity (Fig. 2f). When we increased XMAP215 activity in the extract, we observed that the mean track velocity increased with spindle length whereas microtubule flux velocity, determined by speckle microscopy, was independent of XMAP215 concentration and always smaller than the measured EB1–GFP track velocity. We thus conclude that spindle length correlates linearly with microtubule growth velocities in spindles.

Studies in *Xenopus* eggs and early embryos suggest an upper limit to spindle length[22]. To determine whether the upper length of the spindle is limited by the polymerase activity of XMAP215, we performed a dose–response assay for spindle length in the presence of different XMAP215 concentrations for the wild-type protein and two engineered mutants, TOG1&2AA–GFP and TOG3&4AA–GFP (Fig. 3a). For all proteins, spindle length initially correlated with XMAP215 concentration but subsequently plateaued (Fig. 3b). Interestingly, the spindles plateaued at different lengths depending on the polymerase activity of the mutants. However, for all proteins, spindles approach their maximal length at approximately 200 nM protein. This is the concentration at which XMAP215 works at its maximum rate *in vitro* because it saturates microtubule plus ends[18]. On the basis of our results, we propose that spindle length approaches its maximal length when microtubule plus ends are saturated with the polymerase, and that the upper limit to spindle length is determined, at least in part, by the maximal growth velocity of microtubules.

XMAP215 was previously reported to also affect other parameters of microtubule dynamics, such as microtubule lifetime[23] and nucleation[24–26]. So far, the best approximation for microtubule lifetime in spindles can be obtained by using single-molecule imaging[14]. We assembled spindles in the presence of Fluor647–tubulin at concentrations where approximately 1 in 100,000 tubulin molecules is labelled and imaged spindles over time (Fig. 4a). The assumption is that the appearance of a single fluorescent tubulin particle reflects a tubulin molecule becoming incorporated into a growing microtubule, and its disappearance reflects the release during microtubule depolymerization. We thus refer to the total amount of time between the appearance and disappearance of a tubulin molecule as its lifetime. We determined a mean microtubule lifetime of 18.2 ± 2.1 s (s.e.m. $n = 60$ bins, 17 spindles), which is comparable to published data[14]. However, when we determined the microtubule lifetime for spindles assembled in the presence of different XMAP215 concentrations, we indeed saw that neither the lifetime distribution nor the lifetime itself changed significantly with XMAP215 activity (Fig. 4b). As a control, we depleted XKCM1 (*Xenopus* kinesin catastrophe modulator-1), a microtubule-depolymerizing kinesin-13 (ref. 16), from *Xenopus* egg extracts and show that we can detect changes in microtubule lifetime (Supplementary Fig. S2a,b). Therefore, we conclude that XMAP215 does not affect microtubule lifetime in spindles.

Our data show that modulation of XMAP215 activity does not significantly affect microtubule lifetime within spindles, consistent with other *in vitro* data that show that XMAP215 has little effect

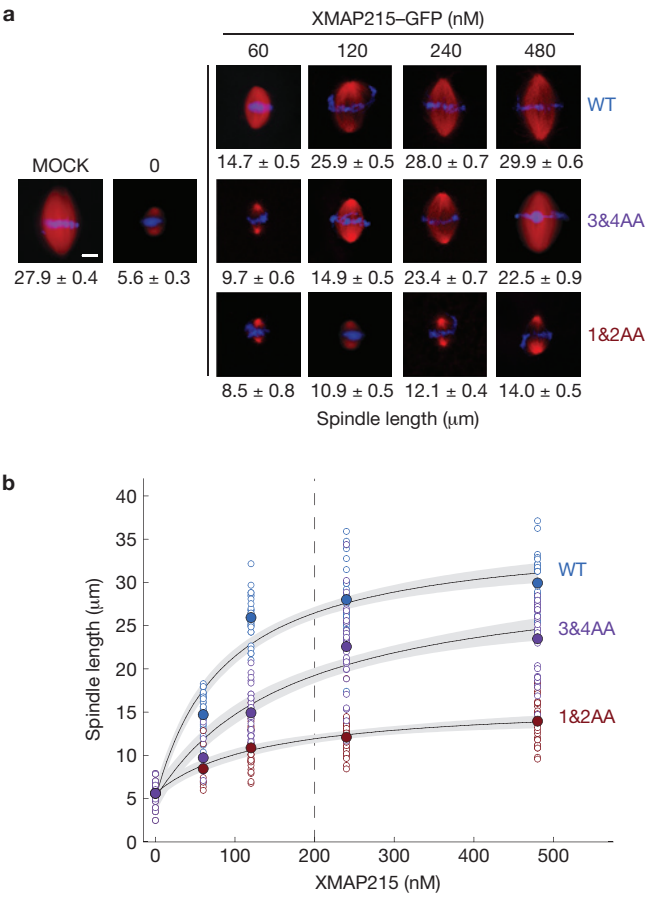

Figure 3 XMAP215 activity limits upper spindle length. (**a**) *Xenopus* egg extract was MOCK or XMAP215 depleted, different concentrations of recombinant wild-type (WT) or mutant XMAP215-GFP were added back and spindles were assembled (red: microtubules, blue: DNA). Scale bar, 10 μm. Average spindle length is indicated (±s.e.m., $n = 30$ spindles assessed over three independent experiments). (**b**) Dose–response curve for spindle length at indicated XMAP215 concentrations for wild-type XMAP215 (blue), and TOG3&4AA (purple) and TOG1&2AA (red) mutants fitted with Michaelis–Menten kinetics. The dashed line indicates the concentration at which all XMAP215 mutants saturate the microtubule plus end *in vitro*. Individual data points (open circles, $n = 30$ spindles assessed over three independent experiments) and the average (filled circles) are shown; the grey areas indicate the 95% confidence intervals of the fitted functions.

on the catastrophe rate[27]. This is not in contradiction with previous *in vitro* studies that show that microtubule lifetime increases with growth velocity[28–30]. In these studies, microtubule growth velocity was increased by changing tubulin concentration and not by modulating the activity of XMAP215, as in our work.

Next, we measured microtubule density over the cross-section at two points within each spindle, halfway between the chromatin and either pole (Fig. 4c, upper row). This measurement resulted in two intensity profiles, from which we evaluated the average local microtubule density for a given spindle (Fig. 4c, middle row). For each XMAP215 concentration, we summarize the density profiles and the respective mean of 15 spindles (Fig. 4c, bottom row), which is roughly constant at any given concentration. Similarly, the total amount of microtubule intensity is independent of XMAP215 activity (Fig. 4d). The variation in intensity along the longitudinal spindle axis, especially

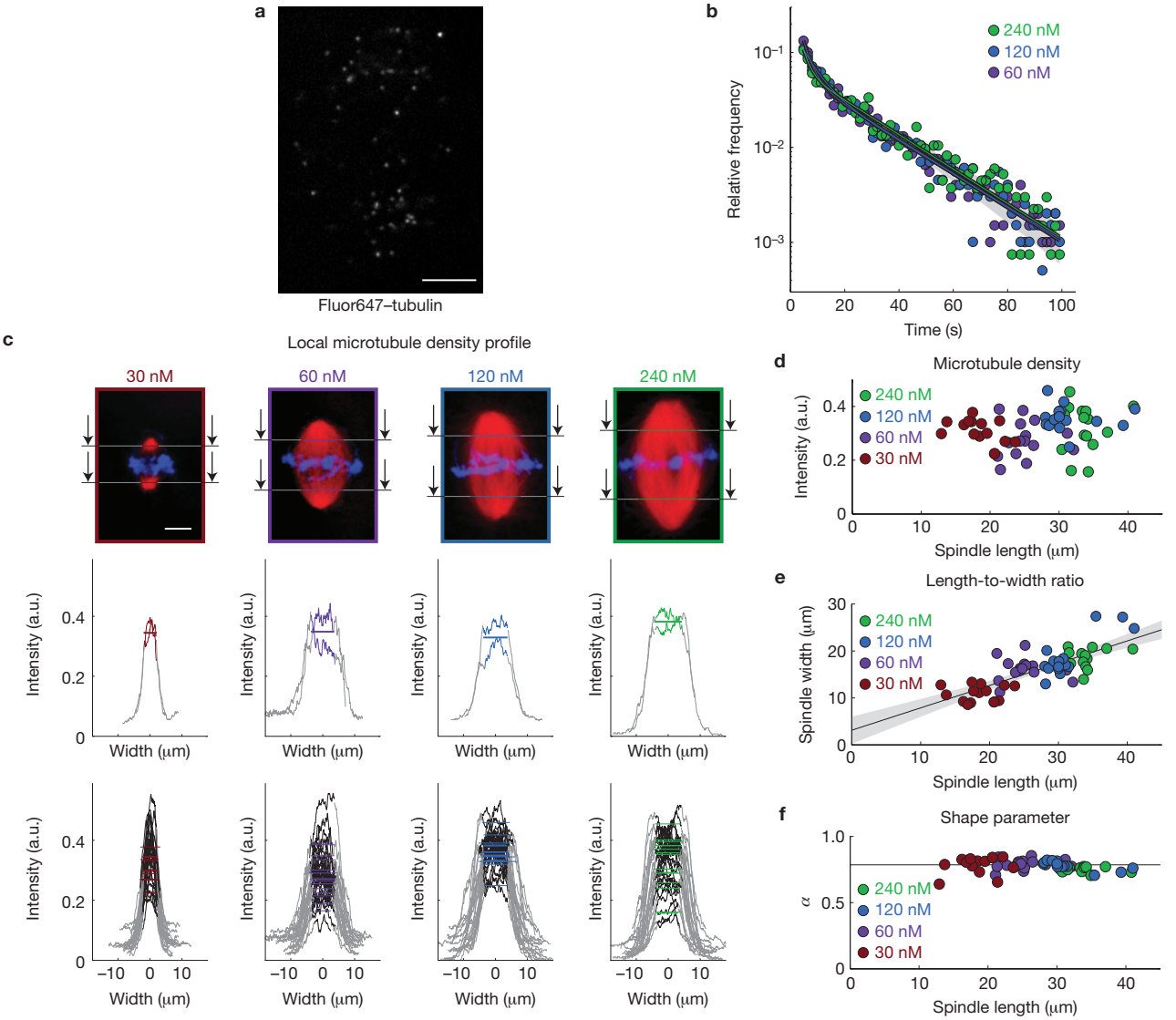

Figure 4 In *Xenopus* spindles, microtubule lifetime, density and spindle shape do not depend on XMAP215 activity. (**a**) Raw single frame of a time-lapse sequence showing single-molecule labelling with Fluor647–tubulin in a *Xenopus* spindle. Scale bar, 10 μm. (**b**) Distribution of tubulin lifetimes in spindles assembled in the presence of 60 nM XMAP215 (purple) with $\tau = 14.9 \pm 1.4$ s (s.e.m., $n = 60$ bins, 1,989 tracks from 12 spindles assessed from 3 independent experiments), 120 nM XMAP215 (blue) with $\tau = 18.2 \pm 2.1$ s (s.e.m., $n = 60$ bins, 1,978 tracks from 17 spindles assessed from 3 independent experiments), and 240 nM XMAP215 (green) with $\tau = 16.9 \pm 2.3$ s (s.e.m., $n = 60$ bins, 1,340 tracks from 12 spindles assessed from 3 independent experiments), all data were fitted with a sum of two exponentials; the grey areas indicate the 95% confidence intervals. (**c**) Spindles were assembled in *Xenopus* egg extract in the presence of different XMAP215 concentrations as indicated. Fluorescence intensity of incorporated Cy3–tubulin was measured along the cross-section as indicated by the arrows (upper row). The profile indicates the fluorescence intensity over the cross-section. The bold coloured line represents the average of the two cross-section scans for a single spindle (middle row). $n = 15$ spindles per XMAP215 concentration (bottom row). Scale bar, 10 μm. (**d**) Microtubule density was estimated by measuring the total fluorescence at the positions $x = \pm 0.25L$ halfway between chromatin and the poles. (**e**) Spindle width was plotted against spindle length and is well described by a linear fit. The grey area indicates the 95% confidence interval of the fitted function. (**f**) The spindle shape parameter was evaluated by defining spindle boundaries using thresholding and evaluating the shape parameter equation (see Methods). The black line represents $\alpha = \pi/4$, the value for an ellipsoidal shape.

in the centre of the spindle, is consistent with volume exclusion by the DNA (Supplementary Fig. S3).

We were further interested in whether XMAP215 affects spindle shape, which is characterized by the length to cross-section ratio as well as the dimensionless shape parameter α, which accounts for cross-section variations over the length of the spindle (Supplementary Note). We show that neither the length-to-width ratio (Fig. 4e) nor the shape parameter α (Fig. 4f) changes with XMAP215 activity. Taken together, our analysis of kinetic and geometric parameters defining spindle length and shape (for spindle volume, see Supplementary Fig. S4) shows that XMAP215 activity predominantly affects microtubule growth velocity in spindles.

We can quantitatively relate the measured parameters (Supplementary Table S1) to the overall spindle length using mass balance. Mass balance is an approach based on the physical principle of mass conservation and describes material fluxes entering and leaving a

system. In *Xenopus* metaphase spindles, which are in steady state, mass balance requires that the rate of tubulin mass entering spindle microtubules by assembly equals the rate of tubulin mass leaving the spindle microtubules by disassembly. In the Supplementary Note, we provide quantitative arguments, incorporating mass balance, that allow us to link microtubule growth velocity to steady-state spindle length L using measured parameters:

$$L = \frac{\beta}{\alpha} v_p \tau^2 W r_0 \frac{\mu}{\rho} \quad (1)$$

Here, v_p is the average microtubule growth velocity, τ is the microtubule lifetime, W is the chromatin width, α is the shape parameter and μ/ρ is the effective cross-section of a microtubule[31]. All of these parameters have been measured (Supplementary Table S1). The only parameters that cannot be observed experimentally are r_0, the chromatin-mediated nucleation rate, and the coefficient β, which accounts for the position dependence of this nucleation[32,33]. Equation (1) predicts that spindle length L is proportional to microtubule growth velocity, if other parameters are constant, exactly as shown experimentally.

An important parameter, which we cannot study experimentally, is the rate and spatial distribution of microtubule nucleation. This limits our ability to show that the only parameter affected by XMAP215 is microtubule growth velocity. Developing a measure of microtubule nucleation in spindles will be particularly important in the future, especially as there are *in vitro* data suggesting that XMAP215 might have an effect on microtubule nucleation[24–26]. It is also known that microtubule nucleation occurs through different pathways, such as chromatin-mediated and microtubule-dependent nucleation. It is so far not possible to experimentally determine the relative contribution of these two different mechanisms to microtubule nucleation in spindles. However, our measured quantities together with equation (1) allow us to estimate the effective microtubule nucleation rate per volume r_0 (Supplementary Table S1). Incorporating different nucleation mechanisms into our analysis further allows us to obtain an upper bound for microtubule-dependent microtubule nucleation (Supplementary Note). This suggests that microtubule-dependent microtubule nucleation cannot be dominant over chromatin-mediated nucleation given the linearity of microtubule growth velocity and spindle length. Indeed, depletion of Augmin, the 8-subunit complex required for microtubule-dependent microtubule nucleation, in *Xenopus* egg extracts causes a reduction in microtubule mass but the overall defects in spindle morphology are modest[34]. Nevertheless, as long as we cannot directly measure microtubule nucleation within spindles, the relative contribution of chromatin-mediated versus microtubule-dependent microtubule nucleation to the overall spindle mass, and the role of XMAP215 in nucleation, remains to be experimentally determined.

In this work, we have systematically modulated the enzymatic activity of the microtubule polymerase XMAP215 to control microtubule growth velocity. We find that spindle length increases linearly with microtubule growth rates in reconstituted *Xenopus* spindles. Furthermore, we show that mass balance applied to microtubules, together with the assumption of constant microtubule density, can be used to link the global property of spindle length to individual microtubule dynamic parameters. On the basis of our experimental work and quantitative arguments, we propose that one organizational principle of setting spindle length is by a balance of non-uniform nucleation and global microtubule disassembly.

Furthermore, our experiments show the power of using a series of mutants whose functions have been tested *in vitro*. This creates an allelic series, which allows the establishment of a quantitative relation between protein function and morphology. One interesting prediction is that spindle length depends quadratically on microtubule lifetime. To test this prediction and thus strengthen the predictive power of our model, it will be important to develop a similar set of reagents that regulate microtubule turnover, such as XKCM1 or Op18, as we have done for XMAP215.

Interestingly, spindle length changes significantly when changing microtubule growth velocity, whereas spindle shape does not (Fig. 4e,f). Indeed, our arguments suggest that we can separate the question of what sets spindle size from what sets spindle shape. We propose that spindle size is determined by mass balance whereas spindle shape is determined by force balance. This would explain previous data showing that microtubule motors do not play an important role in controlling spindle length[8]. For scaling spindle size during development, this separation allows fine-tuning of spindle length without altering gross spindle morphology. The fact that we can separate spindle size and shape is related to the material properties of the spindle. Many observations suggest that spindles can exhibit liquid-crystal-like properties[12,35–39]. Describing spindles as active liquid-crystal-like objects, in which spindle mass is determined by microtubule dynamics parameters, may be a powerful way in the future to link the phenotypes of engineered mutant proteins with the activity of the proteins themselves. □

METHODS

Methods and any associated references are available in the online version of the paper.

Note: Supplementary Information is available in the online version of the paper

ACKNOWLEDGEMENTS

We are grateful to A. Bird, C. Brangwynne, M. Braun, N. Goehring, J. Gopalakrishnan, O. Gruss, G. Salbreux, M. Zanic and D. Zwicker for critical evaluation of the manuscript. We thank all members of the Howard, Hyman and Jülicher laboratories for continuous discussions, H. Andreas for frog care, O. Gruss for the XKCM1 antibody, and Y. Kalaidzidis and M. Chernykh for help with the tracking software. P.O.W. was supported by an EMBO long-term fellowship. J.B. is supported by the European Commission's 7th Framework Programme grant Systems Biology of Mitosis (FP7-HEALTH-2009-241548/MitoSys). S.R. is supported by the European Commission's 7th Framework Programme grant Systems Biology of Stem Cells and Reprogramming (HEALTH-F7-2010-242129/SyBoSS).

AUTHOR CONTRIBUTIONS

This work represents a truly collaborative effort. Each author has contributed significantly to the findings and regular group discussions guided the development of the ideas presented here.

COMPETING FINANCIAL INTERESTS

The authors declare no competing financial interests.

Published online at www.nature.com/doifinder/10.1038/ncb2834
Reprints and permissions information is available online at www.nature.com/reprints

1. Walczak, C. E. & Heald, R. Mechanisms of mitotic spindle assembly and function. *Int. Rev. Cytol.* **265,** 111–158 (2008).
2. Gatlin, J. C. & Bloom, K. Microtubule motors in eukaryotic spindle assembly and maintenance. *Semin. Cell Dev. Biol.* **21,** 248–254 (2010).
3. Kinoshita, K., Arnal, I., Desai, A., Drechsel, D. N. & Hyman, A. A. Reconstitution of physiological microtubule dynamics using purified components. *Science* **294,** 1340–1343 (2001).

4. Brouhard, G. J. *et al.* XMAP215 is a processive microtubule polymerase. *Cell* **132,** 79–88 (2008).
5. Levy, D. L. & Heald, R. Mechanisms of intracellular scaling. *Annu. Rev. Cell Dev. Biol.* **28,** 113–135 (2012).
6. Chan, Y-H. M. & Marshall, W. F. How cells know the size of their organelles. *Science* **337,** 1186–1189 (2012).
7. Goehring, N. W. & Hyman, A. A. Organelle growth control through limiting pools of cytoplasmic components. *Curr. Biol.* **22,** R330–R9 (2012).
8. Goshima, G., Wollman, R., Stuurman, N., Scholey, J. M. & Vale, R. D. Length control of the metaphase spindle. *Curr. Biol.* **15,** 1979–1988 (2005).
9. Burbank, K. S., Mitchison, T. J. & Fisher, D. S. Slide-and-cluster models for spindle assembly. *Curr. Biol.* **17,** 1373–1383 (2007).
10. Loughlin, R., Wilbur, J. D., McNally, F. J., Nédélec, F. J. & Heald, R. Katanin contributes to interspecies spindle length scaling in *Xenopus*. *Cell* **147,** 1397–1407 (2011).
11. Brugués, J., Nuzzo, V., Mazur, E. & Needleman, D. J. Nucleation and transport organize microtubules in metaphase spindles. *Cell* **149,** 554–564 (2012).
12. Shimamoto, Y., Maeda, Y. T., Ishiwata, S., Libchaber, A. J. & Kapoor, T. M. Insights into the micromechanical properties of the metaphase spindle. *Cell* **145,** 1062–1074 (2011).
13. Mitchison, T. J. T. *et al.* Roles of polymerization dynamics, opposed motors, and a tensile element in governing the length of *Xenopus* extract meiotic spindles. *Mol. Biol. Cell* **16,** 3064–3076 (2005).
14. Needleman, D. J. *et al.* Fast microtubule dynamics in meiotic spindles measured by single molecule imaging: evidence that the spindle environment does not stabilize microtubules. *Mol. Biol. Cell* **21,** 323–333 (2010).
15. Yang, G. G. *et al.* Architectural dynamics of the meiotic spindle revealed by single-fluorophore imaging. *Nat. Cell Biol.* **9,** 1233–1242 (2007).
16. Howard, J. & Hyman, A. A. Microtubule polymerases and depolymerases. *Curr. Opin. Cell Biol.* **19,** 31–35 (2007).
17. Al-Bassam, J. & Chang, F. Regulation of microtubule dynamics by TOG-domain proteins XMAP215/Dis1 and CLASP. *Trends Cell Biol.* **21,** 604–614 (2011).
18. Widlund, P. O. *et al.* XMAP215 polymerase activity is built by combining multiple tubulin-binding TOG domains and a basic lattice-binding region. *Proc. Natl Acad. Sci.* **108,** 2741–2746 (2011).
19. Kinoshita, K. Aurora A phosphorylation of TACC3/maskin is required for centrosome-dependent microtubule assembly in mitosis. *J. Cell Biol.* **170,** 1047–1055 (2005).
20. Zanic, M., Stear, J. H., Hyman, A. A. & Howard, J. EB1 recognizes the nucleotide state of tubulin in the microtubule lattice. *PLoS ONE* **4,** e7585 (2009).
21. Maurer, S. P., Fourniol, F. J., Bohner, G., Moores, C. A. & Surrey, T. EBs recognize a nucleotide-dependent structural cap at growing microtubule ends. *Cell* **149,** 371–382 (2012).
22. Wuehr, M. *et al.* Evidence for an upper limit to mitotic spindle length. *Curr. Biol.* **18,** 1256–1261 (2008).
23. Hamada, T., Itoh, T. J., Hashimoto, T., Shimmen, T. & Sonobe, S. GTP is required for the microtubule catastrophe-inducing activity of MAP200, a tobacco homolog of XMAP215. *Plant Physiol.* **151,** 1823–1830 (2009).
24. Popov, A. V., Severin, F. & Karsenti, E. XMAP215 is required for the microtubule-nucleating activity of centrosomes. *Curr. Biol.* **12,** 1326–1330 (2002).
25. Groen, A. C., Maresca, T. J., Gatlin, J. C., Salmon, E. D. & Mitchison, T. J. Functional overlap of microtubule assembly factors in chromatin-promoted spindle assembly. *Mol. Biol. Cell* **20,** 2766–2773 (2009).
26. Slep, K. C. & Vale, R. D. Structural basis of microtubule plus end tracking by XMAP215, CLIP-170, and EB1. *Mol. Cell* **27,** 976–991 (2007).
27. Vasquez, R. J., Gard, D. L. & Cassimeris, L. XMAP from *Xenopus* eggs promotes rapid plus end assembly of microtubules and rapid microtubule polymer turnover. *J. Cell Biol.* **127,** 985–993 (1994).
28. Walker, R. A. *et al.* Dynamic instability of individual microtubules analyzed by video light microscopy: rate constants and transition frequencies. *J. Cell Biol.* **107,** 1437–1448 (1988).
29. Verde, F., Dogterom, M., Stelzer, E., Karsenti, E. & Leibler, S. Control of microtubule dynamics and length by cyclin A- and cyclin B-dependent kinases in *Xenopus* egg extracts. *J. Cell Biol.* **118,** 1097–1108 (1992).
30. Dogterom, M. & Leibler, S. Physical aspects of the growth and regulation of microtubule structures. *Phys. Rev. Lett.* **70,** 1347–1350 (1993).
31. Loughlin, R., Heald, R. & Nedelec, F. A computational model predicts *Xenopus* meiotic spindle organization. *J. Cell Biol.* **191,** 1239–1249 (2010).
32. Hyman, A. & Karsenti, E. The role of nucleation in patterning microtubule networks. *J. Cell Sci.* **111,** 2077–2083 (1998) Pt 15.
33. Gruss, O. J. The mechanism of spindle assembly: functions of Ran and its target TPX2. *J. Cell Biol.* **166,** 949–955 (2004).
34. Petry, S., Pugieux, C., Nédélec, F. J. & Vale, R. D. Augmin promotes meiotic spindle formation and bipolarity in *Xenopus* egg extracts. *Proc. Natl Acad. Sci. USA* **108,** 14473–14478 (2011).
35. Gatlin, J. C., Matov, A., Danuser, G., Mitchison, T. J. & Salmon, E. D. Directly probing the mechanical properties of the spindle and its matrix. *J. Cell Biol.* **188,** 481–489 (2010).
36. Itabashi, T. *et al.* Probing the mechanical architecture of the vertebrate meiotic spindle. *Nat. Methods* **6,** 167–172 (2009).
37. Inoué, S. Microtubule dynamics in cell division: exploring living cells with polarized light microscopy. *Annu. Rev. Cell Dev. Biol.* **24,** 1–28 (2008).
38. Mitchison, T. J. *et al.* Bipolarization and poleward flux correlate during *Xenopus* extract spindle assembly. *Mol. Biol. Cell* **15,** 5603–5615 (2004).
39. Isenberg, I. On the theory of the nematic phase and its possible relation to the mitotic spindle structure. *Bull. Math. Biophys.* **16,** 83–96 (1954).

DOI: 10.1038/ncb2834

METHODS

Spindle assembly in *Xenopus* egg extract. Cytostatic factor (CSF) extracts were prepared from *Xenopus* eggs arrested in metaphase of meiosis II as described previously[40]. To promote bipolar spindle formation, demembranated sperm nuclei were added to the CSF extract, cycling to interphase was induced by the addition of $CaCl_2$ to 0.6 mM and after 90 min the system was rearrested in M-phase using one volume of CSF extract. Spindles were assembled as described above in either MOCK-depleted extracts or in XMAP215-depleted extracts supplemented with XMAP215 buffer, XMAP215–GFP or recombinant XMAP215–GFP mutants to 120 nM or indicated concentrations. For each experiment, 15–60 spindles assessed over three different extracts were analysed (Figs 1b–e, 2a–e, 3a and 4a,c and Supplementary Figs S1a–d and S2a) .

Depletion/add-back experiments and pulldown assays. CSF extract (100 µl) was either MOCK-, XKCM1- or XMAP215-depleted by incubating the CSF extract twice with 20 µl Dynal Protein A beads (Invitrogen) coupled to unspecific rabbit serum IgG, a carboxy-terminal XMAP215 antibody or an antibody against XKCM1, respectively. Depletion efficiency was monitored by functional assays and western blot analysis. The pulldown assay was performed by crosslinking 0.5 µg anti-GFP antibody per microlitre of Dynal Protein G beads (Invitrogen) in the presence of DMP (SIGMA). Recombinant, GFP-tagged proteins or GFP alone was added to CSF extracts and incubated with the anti-GFP beads at 4 °C for 40 min. The beads were washed extensively and eluted with CSF-XB (without sucrose) at pH 7.7, 1 M KCl. The elution was TCA precipitated, separated by SDS gel electrophoresis and analysed by western blotting.

Antibodies. The C-terminal antibody used for XMAP215 depletion from *Xenopus* egg extracts was raised against a peptide containing the last 15 amino acids of XMAP215 and affinity purified against this peptide as described before[24]. For western blot analysis, anti-XMAP215 was used at 5 µg ml^{-1} final concentration. Anti-*Xenopus* TACC3 antibodies were raised and purified against the GST fusion protein that contained an amino-terminal fragment of TACC3 (amino acids 7–208) as described previously[19]. For western blot analysis, anti-TACC3 was used at 3 µg ml^{-1} final concentration. A monoclonal anti-α-tubulin (SIGMA, T5168, Clone B-5-1-2) was used in western blots as a loading control (working dilution 1:5,000). Goat anti-GFP was raised against His-tagged full-length EGFP, affinity-purified with GST-tagged full-length EGFP and used at 50 ng ml^{-1} final concentration. The anti-XKCM1 antibody was a gift from O. Gruss (ZMBH, Germany) and was raised against full-length SUMO-tagged XKCM1. XKCM1 serum (250 µl) was coupled to 100 µl Protein A beads; 2 × 40 µl beads were used to deplete 100 µl CSF extract.

Purification of XMAP215– and EB1–GFP. Wild-type XMAP215–GFP and mutants were expressed in *SF*+ cells using the Bac-to-Bac system (Invitrogen) and purified as described previously[18]. EB1–GFP was expressed and purified as described previously[20].

Porcine tubulin: preparation, labelling and polymerization with GMPCPP. Labelling of cycled tubulin with Cy3 (GE Healthcare) or AlexaFluor488 (Invitrogen) was performed as described previously[41]. Porcine HiLyte Fluor647 tubulin was purchased from Cytoskeleton (# TL670M). GMPCPP microtubules were grown as described previously[42].

Image acquisition and data processing. The total-internal-reflection fluorescence imaging was performed with a set-up described previously[4,18]. Microtubule growth measurements (Fig. 1h,i and Supplementary Fig. S1e,f) were performed in Metamorph (Universal Imaging).

To measure spindle length, shape and microtubule density, the assembled spindles were fixed in the presence of 0.2 mg ml^{-1} Cy3-labelled tubulin and DAPI in squash-fixed samples. Stacks of fixed spindles were acquired in 1-µm steps with a Zeiss LSM 700 laser scanning microscope and a Zeiss LCI Plan-Neofluar ×63, 1.3 NA immersion correction objective using ZEN software. Quantitative analysis of spindle length (Figs 1c,e and 3a,b and Supplementary Fig. S1d) was carried out using a custom algorithm as described before[43]. For quantifying the fluorescence intensity of incorporated Cy3–tubulin, labelled tubulin was added to the extract before the start of the experiment to ensure equal Cy3–tubulin concentrations in controls and all conditions. Images were captured at the same camera setting and further processed using ImageJ. Using the maximum-intensity projection we created an output image from the acquired stack, in which we manually set the threshold level to define the region of interest corresponding to the spindle contours. Using the defined region of interest, the acquired stack and the image processing toolbox in Matlab (Matlab 8.0, The MathWorks), the overall intensity in each plane was evaluated. For further evaluation, the plane with the highest value was selected. The longitudinal spindle axis was determined on the basis of the intensity map. At first, the centroid was computed by weighting with the intensity in the region of interest. With respect to this centroid, the second moments of area, also weighted with the intensity, were evaluated and the first principal axis was taken as the longitudinal and the second as the normal axis. The density profile along the longitudinal axis was then extracted by averaging in the normal direction of this slice. To determine the width of the aligned chromosomes, we stained DNA with DAPI (Supplementary Fig. S3) and analysed the intensity profile in the same coordinate system as the tubulin staining. The spindle shape parameter (Fig. 4f) was evaluated using the boundaries of the region of interest and integrating Supplementary Equation S9 with the trapezoidal rule.

To measure microtubule growth velocities in spindles (Fig. 2), we added EB1–GFP to assembled spindles and imaged every 0.3 s using an Olympus IX71 inverted spinning-disc confocal microscope equipped with a Yokogawa CSU10 scan head, a 488 nm solid-state coherent sapphire (75 mW) laser line, an Andor iXon EM+ DU-897 BV back-illuminated electron-multiplying CCD (charge-coupled device) camera, an Olympus UPlan FluarN 60 × 0.9 objective, and the Andor software. Detection and tracking of EB1–GFP was performed using the Motion Tracking software package (http://motiontracking.mpi-cbg.de; ref 44), written in the Pluk development environment[45]. The coordinates of detected EB1–GFP tracks were used to calculate the end-to-end distance and duration of every track. Then, the EB1–GFP tracks were binned by time and the average distance for each group was evaluated. The weighted linear fit to this evaluated distance versus time data provides the velocity at which the EB1–GFP comets grow in a spindle (Fig. 2c–e).

To measure tubulin turnover and microtubule flux (Figs 4b and 2f), we used tubulin single-molecule imaging[14,46]. Briefly, spindle reactions were supplemented with Fluor647–tubulin to achieve a final concentration of 100 pM and movies were acquired using an Olympus IX81 inverted stand spinning-disc confocal microscope with a Yokogawa CSU-X1 scan head, a 640 nm solid-state laser line (100 mW), an Andor iXon EM+ DU-897 BV back-illuminated electron-multiplying CCD camera, an Olympus UPlanSApo ×60 1.35 NA oil objective, and Andor software. To evaluate the flux velocities, detection and tracking of tubulin speckles as well as the calculations were performed as described for the EB1–GFP tracks. The duration of the individual tracks was used to estimate the lifetime distribution. The lifetime data were fitted, using the fitting toolbox in Matlab (Matlab 8.0, The MathWorks), with a double-exponential function, which corresponds to a case where the number of rescues per microtubule is small[11,47,48]. To control that photobleaching is not significant under our imaging conditions, we analysed the number of objects, their integral intensity and the number of tracks over time (data not shown).

40. Hannak, E. & Heald, R. Investigating mitotic spindle assembly and function *in vitro* using *Xenopus laevis* egg extracts. *Nat. Protoc.* **1,** 2305–2314 (2006).
41. Hyman, A. *et al.* Preparation of modified tubulins. *Methods Enzymol.* **196,** 478–485 (1991).
42. Gell, C. *et al.* Purification of tubulin from porcine brain. *Methods Mol. Biol.* **777,** 15–28 (2011).
43. Reber, S., Over, S., Kronja, I. & Gruss, O. J. CaM kinase II initiates meiotic spindle depolymerization independently of APC/C activation. *J. Cell Biol.* **183,** 1007–1017 (2008).
44. Rink, J., Ghigo, E., Kalaidzidis, Y. & Zerial, M. Rab conversion as a mechanism of progression from early to late endosomes. *Cell* **122,** 735–749 (2005).
45. Kalaidzidis, L. Y., Gavrilov, A. V., Zaitsev, P. V., Kalaidzidis, A. L. & Korolev, E. V. PLUK—an environment for software development. *Prog. Comput. Softw.* **23,** 206–211 (1997).
46. Mirny, L. A. & Needleman, D. J. Quantitative characterization of filament dynamics by single-molecule lifetime measurements. *Methods Cell Biol.* **95,** 583–600 (2010).
47. Wilde, A. *et al.* Ran stimulates spindle assembly by altering microtubule dynamics and the balance of motor activities. *Nat. Cell Biol.* **3,** 221–227 (2001).
48. Brown, K. S. *et al. Xenopus tropicalis* egg extracts provide insight into scaling of the mitotic spindle. *J. Cell Biol.* **176,** 765–770 (2007).

nature cell biology

DOI: 10.1038/ncb2834

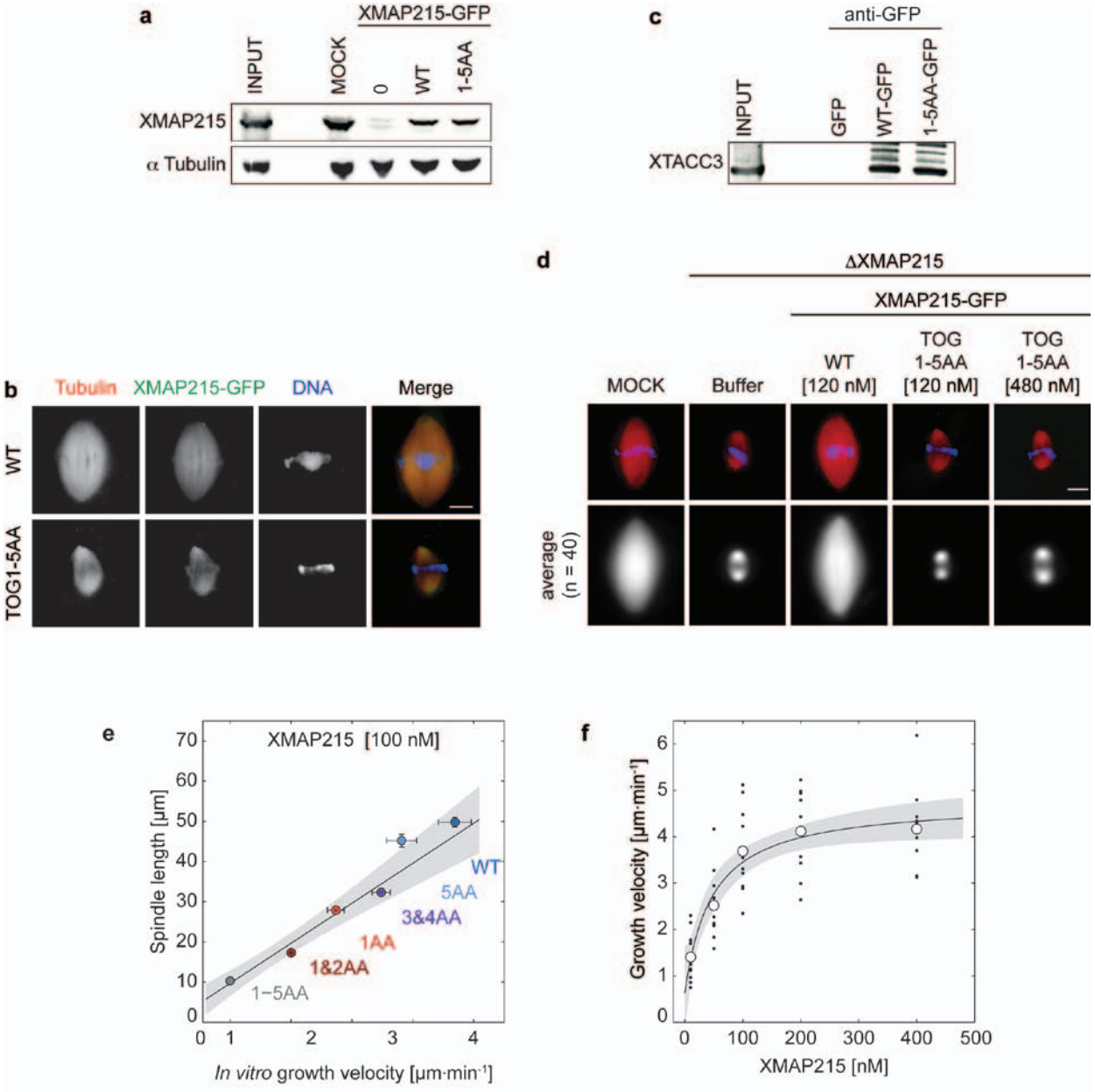

Figure S1 XMAP215 TOG1-5AA binds to spindle microtubules and XTACC3 (**a**) *Xenopus* egg extract was MOCK or XMAP215 depleted, recombinant GFP-tagged XMAP215 wildtype (WT) or TOG1-5AA protein was added back to 120 nM, which is the endogenous concentration. Tubulin was used as a loading control. (**b**) A spindle assembled in XMAP215-depleted *Xenopus* egg extract in the presence of recombinant XMAP215-GFP (WT) or TOG1-5AA-GFP to 120 nM. Although the full mutant XMAP215 TOG1-5AA no longer binds tubulin, it still localizes to spindle microtubules. Note that spindles assembled in the presence of TOG1-5AA are much smaller than wildtype spindles, also at high concentrations. Scale bar: 10 µm (**c**) Pulldown of recombinant proteins from *Xenopus* egg extract on anti GFP-beads, beads eluate was analyzed by Western Blot for the presence of XTACC3. (**d**) Spindles were assembled in the presence of XMAP215 or the full mutant XMAP215 TOG1-5AA at the indicated concentrations. The upper row shows representative spindles (red: microtubules, blue: DNA), the lower row shows an average image of all spindles (n=40, assessed over three independent experiments). Scale bar: 10 µm (**e**) Spindle length (Fig. 1c) plotted versus the *in vitro* microtubule growth velocities promoted by different XMAP215 mutants at 100 nM (as compared to the maximum growth promotion at 400 nM, shown in Fig. 1h). Error bars indicate SE (n_y=40 spindles assessed over 3 independent experiments; n_x = WT 11(2), 5AA 15(2), 3&4AA 11(2), 1AA 11 (2), 1&2AA 15 (2), 1-5 AA no growth. N_x=independent measurements of individual growth events. Number of independent experiments for each condition is given in parentheses.). Grey area indicates the 95% confidence interval of the fitted linear function. (**f**) Microtubule growth velocities measured at different XMAP215 concentrations in a TIRF assay. The mean growth velocity is indicated by open circles, individual data points by dots (n=10 independent measurements of individual growth events), which were fitted with Michaelis-Menten kinetics. Grey area indicates the 95% confidence interval of the fitted function.

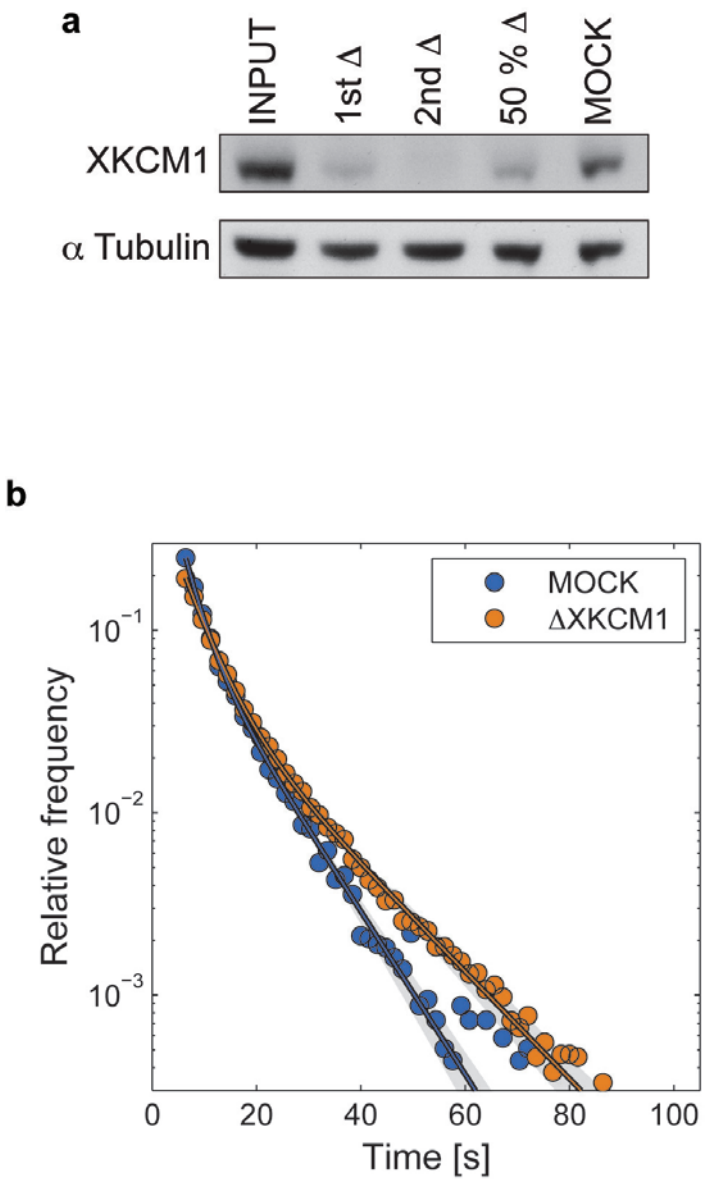

Figure S2 Depleting XKCM1 from *Xenopus* egg extracts increases microtubule lifetime. (**a**) CSF-extract was immuno-depleted of XKCM1 (2ndΔ), one volume of fresh CSF-extract was added back to obtain 50% of endogenous XKCM1 concentration. (**b**) Spindles were assembled in the presence of Fluor647-tubulin and imaged with an Olympus IX81 spinning disc confocal microscope. Distribution of tubulin lifetimes in spindles assembled in control extracts (blue) with (SE, n=60 bins, 13 745 tracks from 12 spindles assessed from 3 independent experiments) and XKCM1-depleted extracts (orange) with (SE, n=60 bins, 63 583 tracks from 13 spindles assessed from 3 independent experiments). All data were fitted with a sum of two exponentials, the grey areas indicate the 95% confidence intervals. Note that the setup of the microscope used to determine the lifetimes in Figure 4b was different (see Methods).

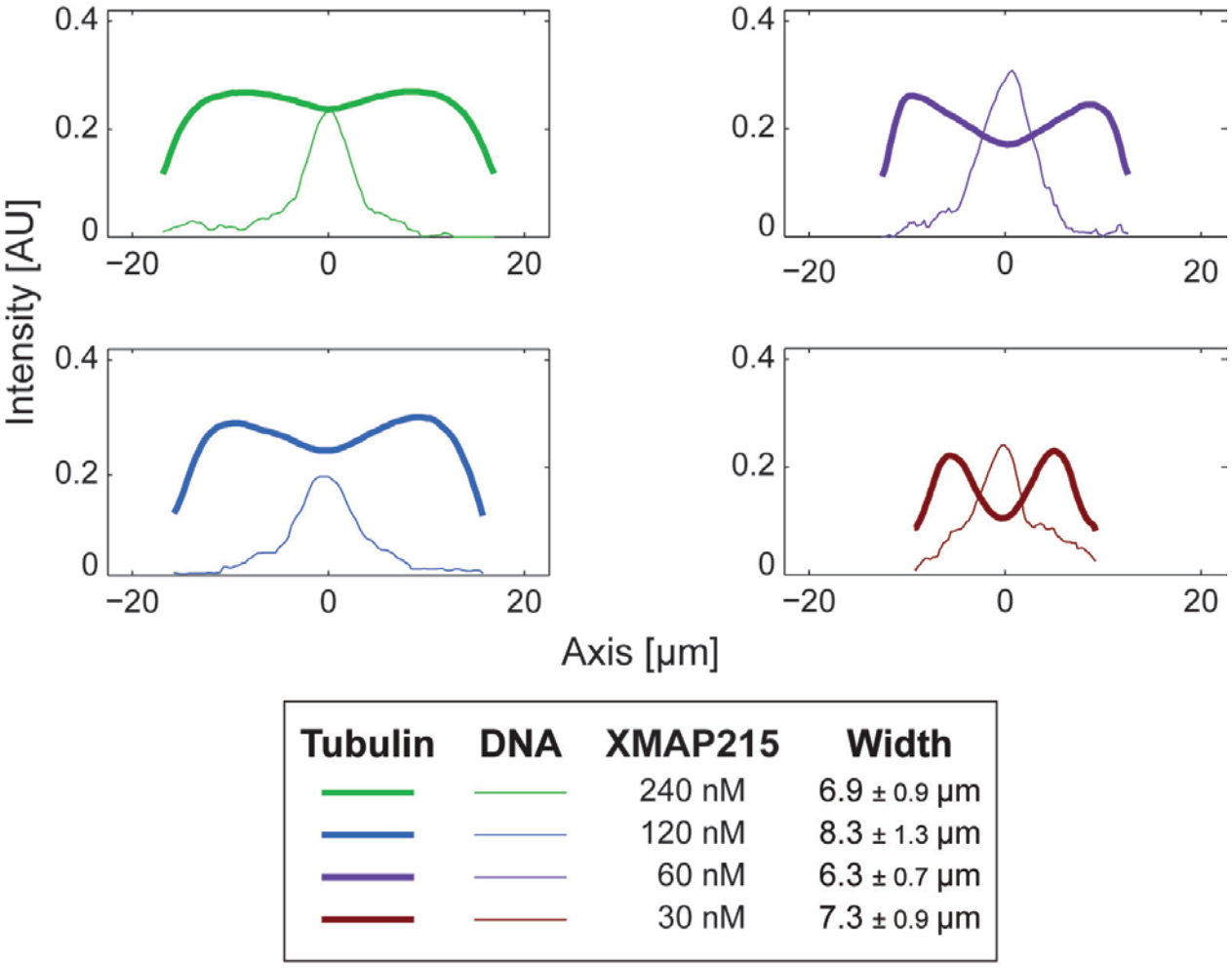

Figure S3 Reduction in microtubule density at the spindle centre is due to volume exclusion by DNA. Microtubule density (bold line) along the longitudinal spindle axis was quantified by the incorporated Cy3-tubulin fluorescence. The variation in intensity along the axis is due to volume exclusion by the DNA, as quantified by the DAPI signal (thin line). The graphs show an average fluorescence intensity of 15 spindles per XMAP215 concentration. The chromatin width was estimated by fitting a Gaussian to the DAPI intensity profiles (SE, n=15 spindles per concentration).

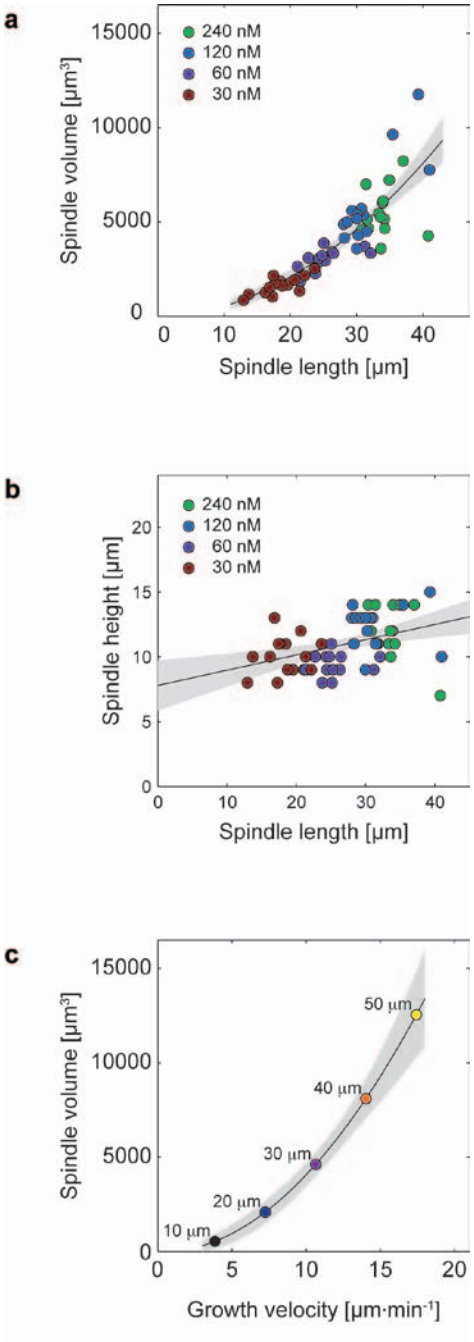

Figure S4 *Spindle volume* (**a**) Individual data points of spindle volume versus spindle length at different XMAP215 concentrations fitted by a power law (exponent: 1.96 ± 0.18 (SE, n=60 spindles assessed over 3 different experiments). (**b**) Individual data points of spindle height versus spindle length at different XMAP215 concentrations fitted by a linear function. (**c**) Spindle volume versus microtubule growth velocity by combing fits from Fig. S4a and 2f. Grey areas indicate the 95% confidence interval of the fitted functions.

Figure 1b Western blot anti XMAP215

Figure 1b Western blot anti α Tubulin

Figure 1d Western blot anti XMAP215

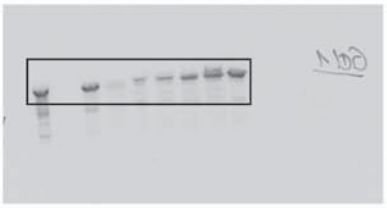

Figure 1d Western blot anti GFP

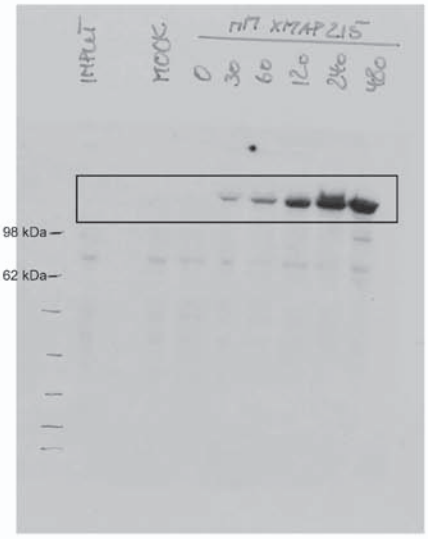

Figure 1d Western blot anti α Tubulin

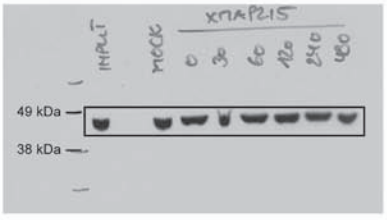

Figure S1a Western blot anti XMAP215

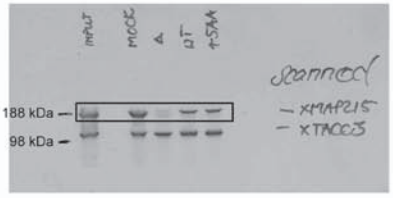

Figure S1c Western blot anti XTACC3

Figure S2a Western blot anti XKCM1

Figure S2a Western blot anti α Tubulin

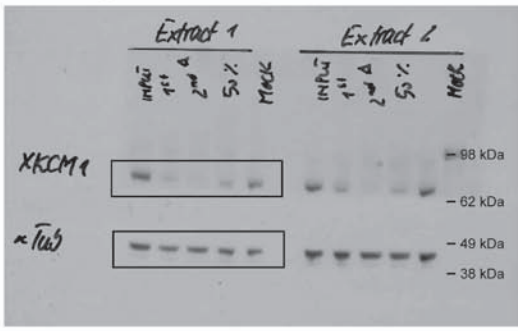

Figure S5 Uncropped Western Blots.

Spindle Parameters

Parameter	*Symbol*	*Value (SE)*	*Unit*	*Reference*
Spindle length	L	39.1 ± 2.2	μm	This study, Figure 2f
Spindle shape parameter	α	0.785	-	This study, Figure 4f
Nucleation profile coefficient	β	2.24	-	This study, Figure S3
Width of nucleation zone	W	8.3 ± 1.3	μm	This study, Supplementary Note
Microtubule cross-section*	a	0.0025	μm^2	Loughlin et al., 2010[10]
Microtubule lifetime	τ	18.2 ± 2.1	s	This study, Figure 4b
Microtubule growth velocity	v_p	12.8 ± 0.9	$\mu m \cdot min^{-1}$	This study, Figure 2f
Nucleation rate per volume	r_0	9.3 ± 2.7	$\mu m^{-3} \cdot s^{-1}$	This study, Equation (1)

* $a = \mu/\rho$ denotes the average area per microtubule in the spindle cross-section.

Supplementary Note

for

XMAP215 activity sets spindle length by controlling the total mass of spindle microtubules

Simone B Reber, Johannes Baumgart, Per O Widlund, Andrei Pozniakovsky, Jonathon Howard, Anthony A Hyman and Frank Jülicher

Mass balance links microtubule dynamics to spindle length

Mass balance allows us to express the total mass M of spindle microtubules in terms of microtubule kinetic parameters that we measured. Spindle volume V follows from spindle mass assuming constant mass density ρ. The spindle geometry is known from the experiments. The only parameter that has not been measured so far is the nucleation rate. In the following we discuss how spindle length L can be related to microtubule kinetic parameters and nucleation rates using mass balance.

Mass balance

In metaphase spindles, mass balance implies that the tubulin mass M_{in} that enters the spindle balances the tubulin mass that accumulates within the spindle and the mass M_{out} that leaves the spindle as

$$\frac{\mathrm{d}M}{\mathrm{d}t} = \frac{\mathrm{d}M_{\mathrm{in}}}{\mathrm{d}t} - \frac{\mathrm{d}M_{\mathrm{out}}}{\mathrm{d}t}, \qquad \text{(S1)}$$

where $\mathrm{d}M_{\mathrm{in}}/\mathrm{d}t$ denotes tubulin influx, $\mathrm{d}M_{\mathrm{out}}/\mathrm{d}t$ tubulin outflux, and t denotes time. Because *Xenopus* metaphase spindles are in steady state, the rate of tubulin mass assembling into spindle microtubules equals the rate of tubulin mass leaving the spindle by disassembly. Therefore, we can represent the microtubule mass balance of a metaphase spindle as

$$\frac{\mathrm{d}M_{\mathrm{in}}}{\mathrm{d}t} = \frac{\mathrm{d}M_{\mathrm{out}}}{\mathrm{d}t}. \qquad \text{(S2)}$$

The tubulin in- and outfluxes are related to microtubule assembly and disassembly as is described in the following.

First, we consider tubulin influx. Tubulin mass enters the spindle by microtubule growth, which is triggered by nucleation. By combining the total number of microtubules nucleated per unit time $\mathrm{d}N/\mathrm{d}t$ with the average microtubule mass generated by growth m, the overall rate at which microtubule mass is added to the spindle reads

$$\frac{\mathrm{d}M_{\mathrm{in}}}{\mathrm{d}t} = m\frac{\mathrm{d}N}{\mathrm{d}t}, \tag{S3}$$

where

$$m = v_{\mathrm{p}}\,\tau\,\mu\,. \tag{S4}$$

Here, v_{p} is the average microtubule growth velocity (Supplementary Note Fig. 1), τ is the average microtubule lifetime, and μ denotes the microtubule mass per length. Note that $v_{\mathrm{p}}\,\tau$ is an estimate of the average microtubule length.

We next consider tubulin outflux. Tubulin mass leaves the spindle by microtubule disassembly throughout the spindle[1]. Thus, the rate of tubulin loss is

$$\frac{\mathrm{d}M_{\mathrm{out}}}{\mathrm{d}t} = \frac{M}{\tau} \tag{S5}$$

where τ is the average microtubule lifetime.

Combining tubulin influx and outflux, the steady-state spindle mass reads

$$M = \frac{\mathrm{d}N}{\mathrm{d}t}\,v_{\mathrm{p}}\,\tau^2\,\mu\,. \tag{S6}$$

Spindle volume

Spindle mass M is related to spindle volume V by $M = \rho\,V$, where ρ is the microtubule mass density within the spindle (Supplementary Note Fig. 2). For our purposes, the important quantity is spindle length. Spindle length L can be obtained from spindle volume and the spindle cross-section area $A(x)$. The cross-section area $A(x)$ is a function of the distance x from the spindle centre with $-L/2 \le x \le L/2$ where L is the spindle length (Supplementary Note Fig. 3). At the spindle tips, the cross section vanishes: $A(\pm L/2) = 0$. Introducing the dimensionless function $f(s)$ with $f(0) = 1$ and $f(\pm 1/2) = 0$, the spindle shape can be described as

$$A(x) = A_0\,f(x/L) \tag{S7}$$

with $s = x/L$ and A_0 denoting the cross-section area in the spindle centre. The spindle volume is given by

$$V = \int_{-L/2}^{L/2} \mathrm{d}x\, A(x) = \alpha\, A_0\, L \qquad \text{(S8)}$$

where

$$\alpha = \int_{-1/2}^{1/2} \mathrm{d}s\, f(s) \qquad \text{(S9)}$$

is a dimensionless number that characterizes spindle shape, independent of the aspect ratio of the spindle, which is defined as $L/\sqrt{A_0}$.

Chromatin-dependent microtubule nucleation

The rate of chromatin-dependent microtubule nucleation in the spindle can be written as

$$\frac{\mathrm{d}N_0}{\mathrm{d}t} = \int_{-L/2}^{L/2} \mathrm{d}x\, A(x)\, r(x)\,. \qquad \text{(S10)}$$

Where $r(x)$ is the nucleation rate per unit volume at distance x from the centre. Microtubules nucleate predominantly in the vicinity of chromatin, which provides a signalling gradient[2,3]. For simplicity, we choose localized nucleation with a Gaussian profile of local nucleation rate per volume

$$r(x) = r_0 \exp\left(-2\,\frac{x^2}{W^2}\right). \qquad \text{(S11)}$$

The characteristic width of the nucleation zone is denoted W. The profile (S11) describes effects of a nucleation-promoting signal near the chromatin, where r_0 is the maximal nucleation rate per volume. The rate of chromatin-mediated nucleation can be written as

$$\frac{\mathrm{d}N_0}{\mathrm{d}t} = \beta\, W A_0\, r_0 \qquad \text{(S12)}$$

where

$$\beta = \frac{L}{W}\int_{-1/2}^{1/2} \mathrm{d}s\, f(s) \exp\left(-2\, s^2\, \frac{L^2}{W^2}\right) \qquad \text{(S13)}$$

is a coefficient that depends on the spindle shape and the nucleation profile.

Spindle length

We first ignore the effects of microtubule-dependent microtubule nucleation $\mathrm{d}N/\mathrm{d}t = \mathrm{d}N_0/\mathrm{d}t$. Using the expressions (S6) and (S8) together with the nucleation rate (S12), the steady-state spindle length is

$$L = \frac{\beta}{\alpha}\, W\, \tau^2\, r_0\, v_\mathrm{p} \frac{\mu}{\rho}\,. \qquad \text{(S14)}$$

Here, μ/ρ is the average area per microtubule in the spindle cross section[4].

Equation (S14) predicts that spindle length is directly proportional to the microtubule growth velocity v_p, to the width W of the region in which microtubules nucleate, and to the nucleation rate r_0. Using the measured parameters (Supplementary Table 1), we can estimate the effective nucleation rate per volume $r_0 = 9.3 \pm 2.7\ \mu\mathrm{m}^{-3} \cdot \mathrm{s}^{-1}$. Furthermore equation (S14) predicts that spindle length L depends quadratically on the average microtubule lifetime τ. This strong dependence on lifetime results from the fact that an increased microtubule lifetime increases both the incorporated microtubule mass per nucleation event and the time over which this mass contributes to spindle mass.

Microtubule-dependent microtubule nucleation

Next, we incorporate effects of microtubule-dependent microtubule nucleation. A single chromatin-mediated nucleation event is followed by subsequent microtubule-dependent nucleation events, creating on average $n = r_\mathrm{l}\, v_\mathrm{p}\, \tau^2$ additional microtubules. Here, r_l is the rate of microtubule-dependent nucleation per unit microtubule length. Since subsequent nucleations create new microtubules that themselves can serve as nucleators and so on, the total nucleation rate becomes $\mathrm{d}N/\mathrm{d}t = (1 + n + n^2 + \cdots)\, \mathrm{d}N_0/\mathrm{d}t$. This can be expressed as $\mathrm{d}N/\mathrm{d}t = (1-n)^{-1}\, \mathrm{d}N_0/\mathrm{d}t$ or

$$\frac{\mathrm{d}N}{\mathrm{d}t} = \frac{1}{1 - r_\mathrm{l}\, v_\mathrm{p}\, \tau^2} \frac{\mathrm{d}N_0}{\mathrm{d}t} \qquad \text{(S15)}$$

combining this with equations (S6), (S8), and (S12) we find

$$L = \frac{\beta}{\alpha} W \tau^2 r_{\mathrm{eff}} v_{\mathrm{p}} \frac{\mu}{\rho} , \qquad \text{(S16)}$$

which has the same form as equation (S14), but with an effective nucleation rate per volume

$$r_{\mathrm{eff}} = \frac{r_0}{1 - r_{\mathrm{l}} v_{\mathrm{p}} \tau^2} , \qquad \text{(S17)}$$

which accounts for the effects of both chromatin-mediated and microtubule-dependent nucleation. Note that r_{eff} depends on the polymerization velocity v_{p}. Thus, spindle length as described by equation (S16) could become a nonlinear function of v_{p} if microtubule-dependent nucleation occurred at a significant rate r_{l}.

The experimentally observed linear relationship, however, provides an upper bound on the value of the microtubule-dependent nucleation rate $r_{\mathrm{l}} \ll 1/(v_{\mathrm{p}} \tau^2)$ and implies that chromatin-mediated nucleation dominates $r_{\mathrm{eff}} \approx r_0$. Fitting the relation (S16) to the observed spindle length as a function of v_{p} (Supplementary Note Fig. 4) provides an upper bound on the value of the microtubule-dependent nucleation rate per unit length $r_{\mathrm{l}} \leq 0.0004\ \mu\mathrm{m}^{-1} \cdot \mathrm{s}^{-1}$ and a corresponding chromatin-mediated nucleation rate per volume $r_0 = 8.5 \pm 2.6\ \mu\mathrm{m}^{-3} \cdot \mathrm{s}^{-1}$.

Figures

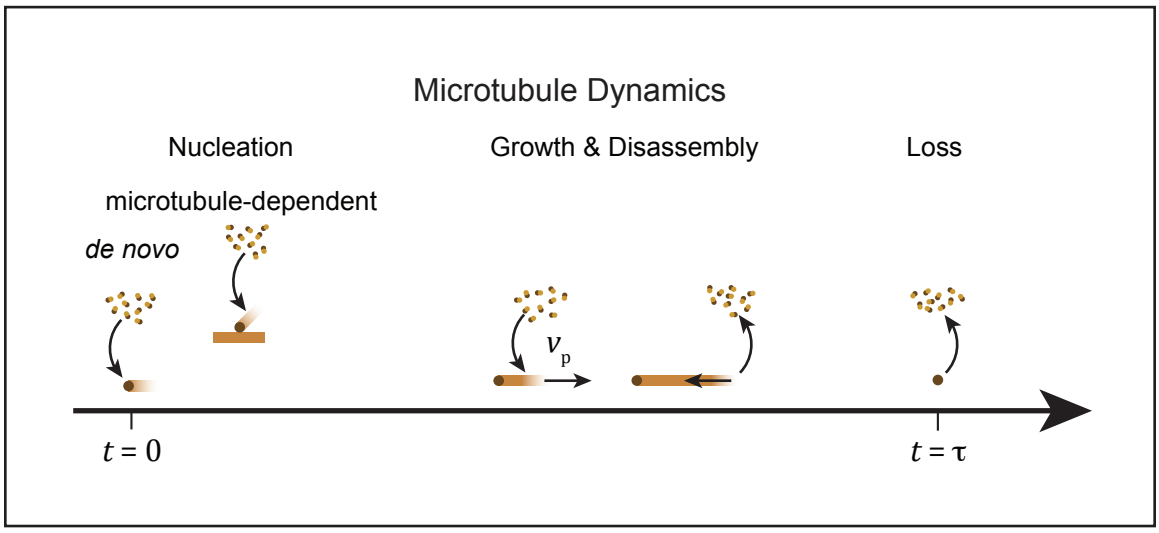

Supplementary Note Figure 1 Schematic depicting key parameters of microtubule dynamics. v_p: Microtubule growth velocity. τ: Microtubule lifetime.

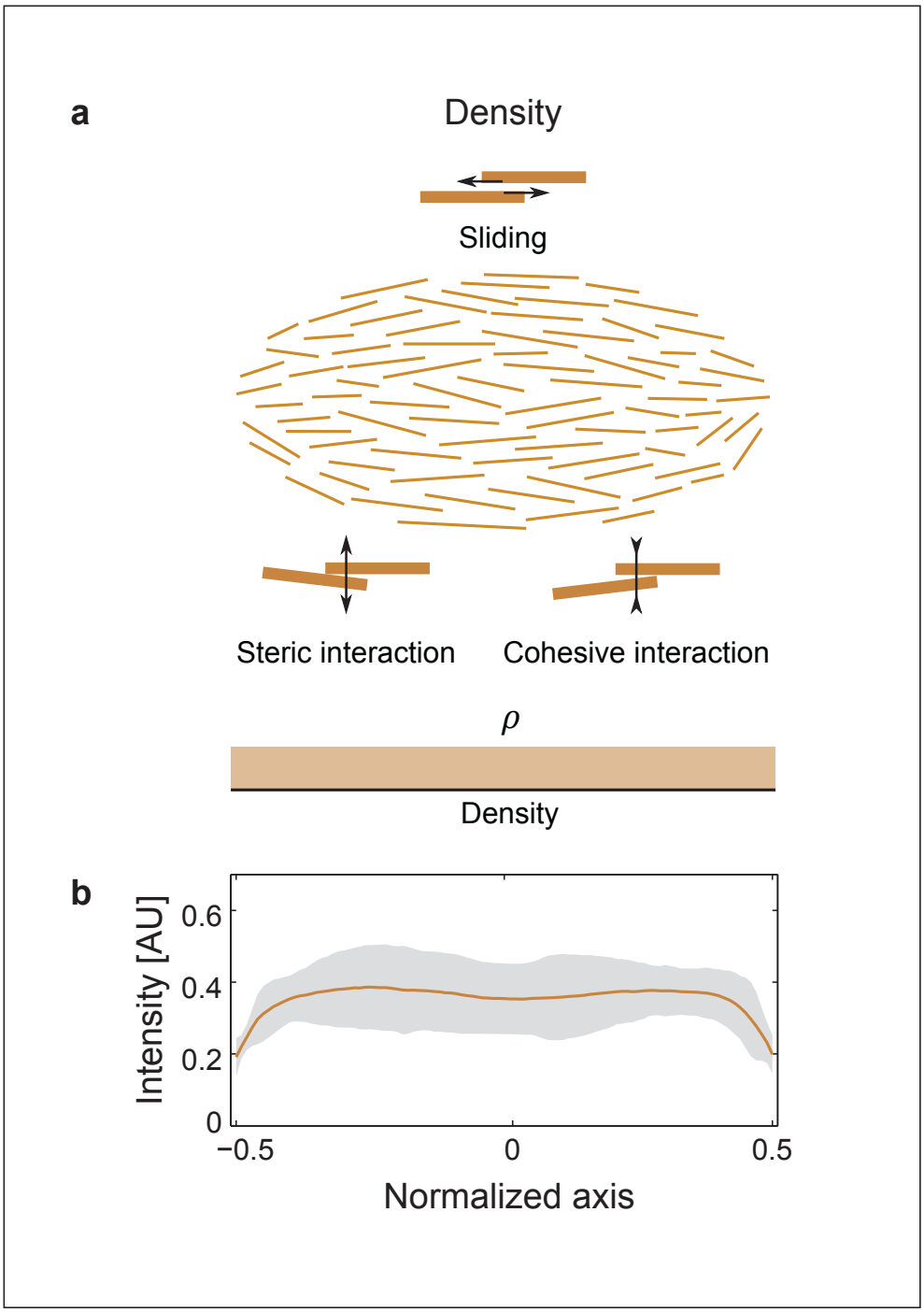

Supplementary Note Figure 2 Due to the liquid-like properties of spindle material microtubule density ρ is constant. On a molecular level this is driven by intermolecular interactions by cross-linking proteins and motors. (**e**) Microtubule density along the spindle pole-to-pole axis measured by Cy3-tubulin incorporation. Brown line shows the average of 15 spindles, the grey area indicates the interval of two standard deviations.

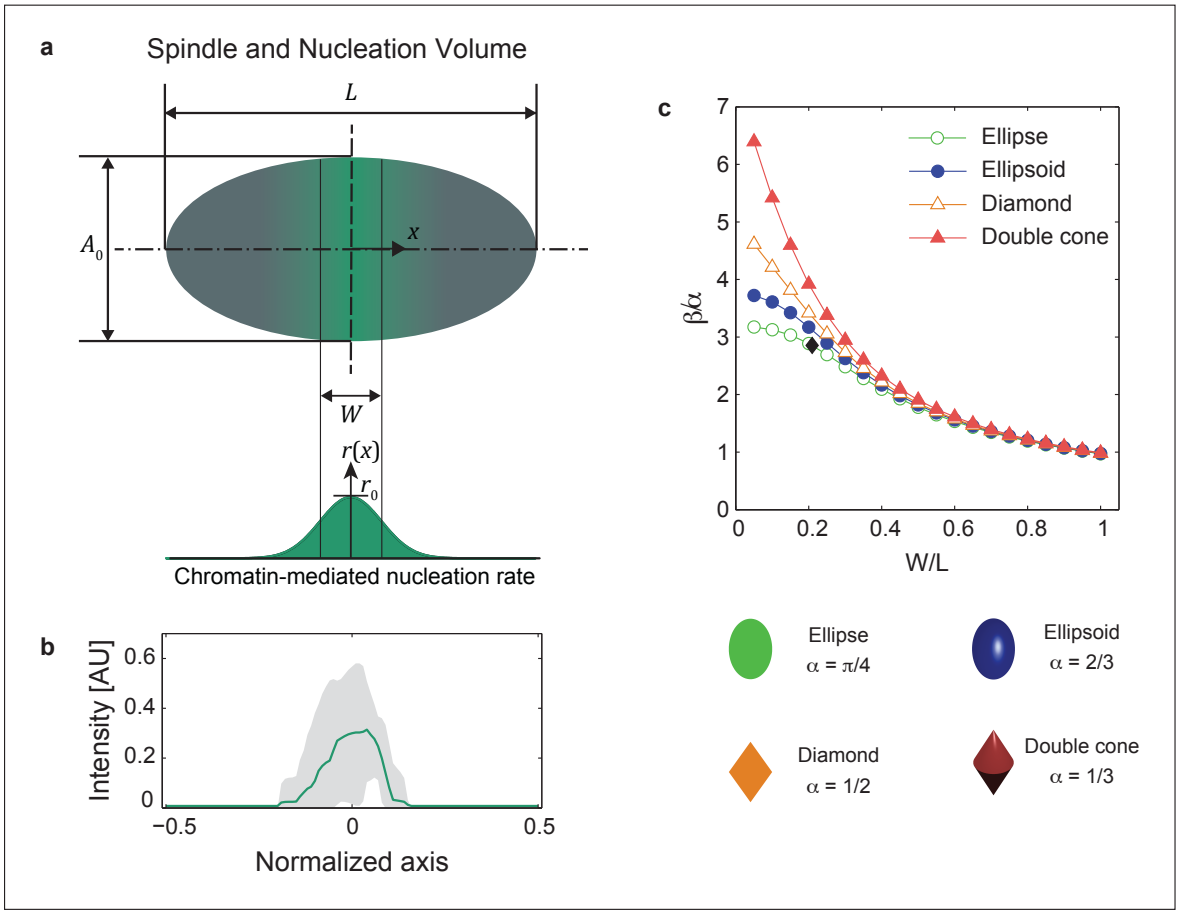

Supplementary Note Figure 3 (**a**) The spindle volume V is defined by $\alpha\, L\, A_0$, with a dimensionless coefficient α (equation S9), spindle length L and the spindle cross-section A_0. The nucleation volume $A_0\, W$ is described by the spindle cross-section A_0 and the width W of the nucleation zone. Nucleation occurs predominately in the vicinity of chromatin at a given rate per volume r_0. (**b**) Width of the nucleation zone as determined by fluorescent DAPI staining. Green line shows the average of 15 spindles, the grey area indicates the interval of two standard deviations. (**c**) Shape and nucleation profile parameters α and β (equation S9 and S13) of simple geometries. Parameters representing the shape and the nucleation profile for different geometries. Black diamond indicates β/α measured for a typical Xenopus wildtype spindle with $W/L = 0.21$ and an elliptical shape.

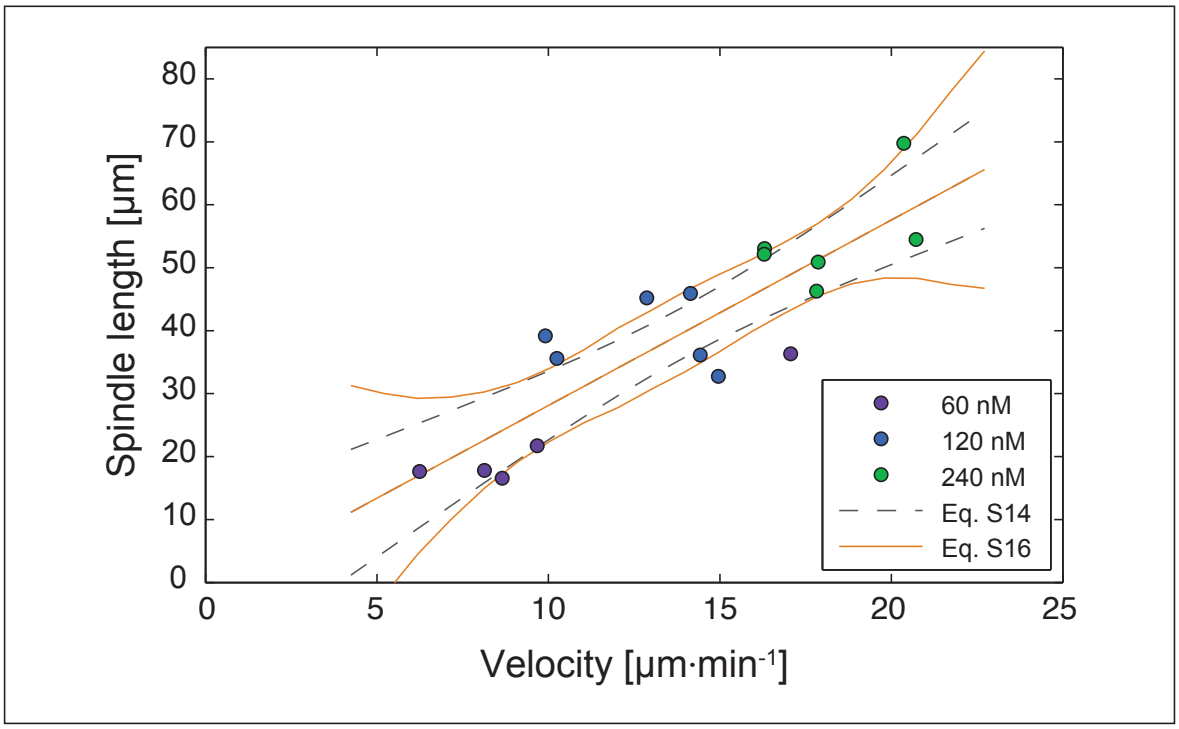

Supplementary Note Figure 4 Fitting the spindle length versus microtubule growth data with equation S16 (orange line) provides an upper bound on the value of the microtubule-dependent nucleation rate per unit length. For comparison the fit with confidence intervals is also given for the model without microtubule-dependent nucleation (equation S14, dashed black line).

References

1. Brugués, J., Nuzzo, V., Mazur, E. & Needleman, D. J. Nucleation and transport organize microtubules in metaphase spindles. *Cell* **149,** 554–564 (2012).
2. Hyman, A. & Karsenti, E. The role of nucleation in patterning microtubule networks. *J Cell Sci* **111 (Pt 15),** 2077–2083 (1998).
3. Gruss, O. J. The mechanism of spindle assembly: functions of Ran and its target TPX2. *J Cell Biol* **166,** 949–955 (2004).
4. Loughlin, R., Heald, R. & Nedelec, F. A computational model predicts Xenopus meiotic spindle organization. *J Cell Biol* **191,** 1239–1249 (2010).